

Subcycling of particle orbits in variational, geometric electromagnetic particle-in-cell methods

Eero Hirvijoki,¹ Katharina Kormann,^{2,3} and Filippo Zonta¹

¹*Department of Applied Physics, Aalto University, P.O. Box 11100, 00076 AALTO, Finland^{a)}*

²*Max-Planck-Institut für Plasmaphysik, Boltzmannstraße 2, 85748 Garching, Germany*

³*Technische Universität München, Department of Mathematics, Boltzmannstraße 3, 85748 Garching, Germany*

(Dated: 19 May 2020)

This paper introduces two subcycling algorithms for particle orbits in variational, geometric particle-in-cell methods addressing the Vlasov–Maxwell system in magnetized plasmas. The purpose of subcycling is to allow different time steps for different particle species and ideally time steps longer than the electron gyroperiod for the global field solves while sampling the local cyclotron orbits accurately. Both our algorithms retain the electromagnetic gauge invariance of the discrete action, guaranteeing a local charge conservation law, and the variational approach provides a bounded long-time energy behavior. In the first algorithm, the global field solves are explicit and the local particle push implicit for each particle individually. The requirement for gauge invariance, however, leads to a peculiarity in the particle push: the magnetic field is orbit-averaged but the effect of the electric field is evaluated only once during the subcycling period. Numerical tests then indicate a possibility of artificial oscillations if the relative electric field impulse on the particles grows large. The second algorithm is proposed to remedy the possible issues of the first algorithm. It is observed that both the magnetic and electric impulses on particle motion can be orbit-averaged if also the electrostatic part of the field-particle interaction term in the discrete action is line-integrated. In numerical experiments, the artificial oscillations are observed to vanish but, at the same time, the algorithm implicitly couples the electric field and the particle push. It remains to be seen whether properly orbit-averaged, yet explicit subcycling algorithms exist within the variational geometric particle-in-cell framework.

I. INTRODUCTION

During the past decade, both understanding and developing of structure-preserving algorithms for simulating plasmas have leaped forward and, to a large extent, this development has been driven by the so-called geometric particle-in-cell (GEMPIC) methods^{1–11}—see¹² for a review of the broader topic and the exhaustive list of references therein referring to GEMPIC methods. Based on discretizing either the underlying variational or Hamiltonian structure, GEMPIC algorithms provide long-time fidelity and stability for models with possibly billions of degrees of freedom. This is especially important for kinetic simulations of magnetized fusion plasmas where reaching macroscopic transport at time scales of 10^{-6} s requires a breathtaking number of time steps to resolve the electron cyclotron motion typically appearing at the time scales of 10^{-11} s. Such an enormous feat has been performed only very recently¹¹ but this will likely become common place during 2020s.

To our knowledge, the GEMPIC methods have so far considered only synchronous integration of particle orbits and electromagnetic fields, whereas the non-GEMPIC methods, that have become the industry standard^{13–21}, implement so-called subcycling or orbit-averaging of par-

tic orbits out of the box. The only GEMPIC attempt in this direction, reported in²², is based on an energy-conserving temporal discretization rather than a variational integrator. Especially in simulating multi-component, strongly magnetized plasmas, treating both ions and electrons kinetically, multiple different time scales naturally emerge as the ion and electron cyclotron periods differ by the respective mass ratio. It would be preferable not to restrict the field solve or the ion push to the fastest time scale—typically the electron cyclotron period unless the plasma density is very high, in which case the electron plasma oscillations become dominant—but to allow for subcycling of particle orbits at their naturally occurring frequencies. The absence of this feature from the GEMPIC methods does not need to remain the state of the business, though, and the purpose of this paper is to take the first steps in modifying GEMPIC methods towards fully asynchronous and, in future, possibly temporally adaptive integration.

We introduce two different candidates for implementing subcycling of particle orbits within the variational GEMPIC framework. Both algorithms retain the electromagnetic gauge invariance of the discrete action—guaranteeing a local charge conservation law—and the variational approach provides a bounded long-time energy behavior. Our first algorithm is intended for upgrading the existing variational GEMPIC methods to include subcycling with minimal effort invested in modifications: the global field solves are explicit and the local particle

^{a)}Electronic mail: eero.hirvijoki@gmail.com

push implicit for each particle individually, just as in the pioneering paper¹. We anticipate that the scheme could be made fully explicit if rectilinear meshes and the novel zigzag path are exploited as, e.g., in¹⁰. The requirement for gauge invariance, however, leads to a peculiar sub-cycling scheme where the magnetic field is orbit-averaged and the effect of electric field on the particle orbits is evaluated only once during the sub-cycling period. Numerical tests with this algorithm indicate that artificial oscillations may occur if the electric field impulse on the particle orbit is too large: in an electrostatically dominated case we observe such modes but in an electromagnetically dominated test we do not. This behavior is likely credited to the electric field not being orbit-averaged the same way as the magnetic field is which increases the instantaneous relative impulse from the electric field in comparison to the impulse from the magnetic field. Indeed, the oscillations are observed to vanish if orbit-averaging is enforced also for the electric field but then the particle push is no longer variational. It appears that measures more radical than quickly modifying existing schemes are worth investigating.

Our second algorithm is proposed to remedy the issues possibly occurring with the semi-explicit algorithm. Instead of relying on the “summation-by-parts” trick as in the traditional variational GEMPIC methods, we observe that enabling proper partial integration in the field–particle-interaction term of the discrete action, both magnetic and electric field impulses can be orbit-averaged, the gauge invariance and consequently the charge conservation retained, while the total algorithm remains variational. Indeed, repeating the numerical tests confirms our hypothesis that the artificial oscillations are rooted in not orbit-averaging the electric field impulse: the scheme does not exhibit such artificial oscillations. The choice of enabling proper partial integration in the discrete action, however, appears to always lead to an implicit scheme, in contrast to the clever summation-by-parts trick that admits explicit field solve. This implicitness, however, only relates to how the electric field, the current density, and the particle push are coupled for the Faraday equation remains explicit. Consequently, both our algorithms have CFL-conditions on the field solves. Per our findings, it remains to be seen if proper orbit-averaging could be performed within the variational framework with explicit schemes.

We will begin by briefly recapping the essential elements of a structure-preserving variational discretization of the Vlasov–Maxwell system in Sec. II, and then proceed to presenting the new algorithms. The semi-explicit scheme is introduced in Sec. III together with the numerical experiments indicating the possible oscillation problem and a demonstration that brute-force orbit-averaging the electric field removes them. Building on this learning outcome, the fully implicit scheme is derived in Sec. IV and the numerical tests repeated, demonstrating that the artificial oscillations no longer exist. Finally, we engage in a brief discussion regarding

the high-performance-computing aspects and stability of the algorithms in Sec. V while the results are summarized and possible suggestions for future research directions discussed in Sec. VI.

II. ELEMENTS OF STRUCTURE-PRESERVING DISCRETIZATION

In this section, we briefly summarize some of the essential building blocks for implementing a variational GEMPIC method for the Vlasov–Maxwell system. For more details, we refer the reader to the excellent papers^{1,9,10}.

Let us assume we have some domain $\Omega \subset \mathbb{R}^3$ and a finite-dimensional discretization of the associated de Rham complex: we expect there to be the sets of scalar and vector valued basis functions $\{W_i^0\}_i$, $\{W_j^1\}_j$, $\{W_k^2\}_k$, and $\{W_\ell^3\}_\ell$, all functions of position \mathbf{x} , such that

$$\nabla W_i^0(\mathbf{x}) = \text{grad}_i^j W_j^1(\mathbf{x}), \quad (1)$$

$$\nabla \times W_j^1(\mathbf{x}) = \text{curl}_j^k W_k^2(\mathbf{x}), \quad (2)$$

$$\nabla \cdot W_k^2(\mathbf{x}) = \text{div}_k^\ell W_\ell^3(\mathbf{x}), \quad (3)$$

where grad_i^j , curl_j^k , and div_k^ℓ denote the elements of the discrete gradient, curl, and divergence matrices, respectively. Einstein summation over the repeated superscript-subscript index pairs is assumed throughout, and the letters i, j, k, ℓ always refer to the corresponding element spaces as denoted above. A typical way to construct such basis is via the Whitney interpolating functions on simplicial meshes.

Because the basis functions satisfy the de Rham complex, we have that

$$0 = \nabla \times \nabla W_i^0 = \text{grad}_i^j \nabla \times W_j^1 = \text{grad}_i^j \text{curl}_j^k W_k^2, \quad (4)$$

$$0 = \nabla \cdot \nabla \times W_j^1 = \text{curl}_j^k \nabla \cdot W_k^2 = \text{curl}_j^k \text{div}_k^\ell W_\ell^3, \quad (5)$$

for all $\mathbf{x} \in \Omega$, implying the matrix identities $\text{curl}_j^k \text{grad}_i^j = 0$ and $\text{div}_k^\ell \text{curl}_j^k = 0$. The spatial discretizations of the vector and scalar potential are then taken to be

$$\mathbf{A}_{\text{ext}}(\mathbf{x}) = a_{\text{ext}}^j W_j^1(\mathbf{x}), \quad (6)$$

$$\mathbf{A}(\mathbf{x}, t) = a^j(t) W_j^1(\mathbf{x}), \quad (7)$$

$$\phi(\mathbf{x}, t) = \phi^i(t) W_i^0(\mathbf{x}), \quad (8)$$

where the subscript “ext” refers to a static, given quantity, and the definitions then imply the following expressions for the finite-dimensional electric and magnetic fields

$$\mathbf{E} = (-\dot{a}^j - \phi^i \text{grad}_i^j) W_j^1 \equiv e^j W_j^1, \quad (9)$$

$$\mathbf{B} = a^j \text{curl}_j^k W_k^2 \equiv b^k W_k^2. \quad (10)$$

A possible external, fixed magnetic field is naturally denoted by

$$\mathbf{B}_{\text{ext}} = a_{\text{ext}}^j \text{curl}_j^k W_k^2 \equiv b_{\text{ext}}^k W_k^2. \quad (11)$$

The finite-dimensional magnetic field now satisfies the identities

$$\partial_t \mathbf{B} = \dot{a}^j \text{curl}_j^k \mathbf{W}_k^2 = -e^j \nabla \times \mathbf{W}_j^1 = -\nabla \times \mathbf{E}, \quad (12)$$

$$\partial_t \nabla \cdot \mathbf{B} = \dot{a}^j \text{curl}_j^k \text{div}_k^\ell \mathbf{W}_\ell^3 = 0, \quad (13)$$

meaning that, if the degrees of freedom for \mathbf{B} initially satisfy $b^k \text{div}_k^\ell = 0$, the magnetic field will stay divergence free for all times.

In particle-in-cell methods, the idea is to let marker particles to carry the phase-space density forward in time, starting from a fixed initial density distribution

$$F_0 = \sum_p \delta(\mathbf{x}_0 - \mathbf{x}_p(t_0)) \delta(\mathbf{v}_0 - \dot{\mathbf{x}}_p(t_0)), \quad (14)$$

where $(\mathbf{x}_p(t_0), \dot{\mathbf{x}}_p(t_0))$ are the initial position and velocity coordinates for the marker trajectory $(\mathbf{x}_p(t), \dot{\mathbf{x}}_p(t))$. In practice, every marker should be weighted with a label w_p accounting for the number of real particles the marker represents. Here we have, however, suppressed this factor for notational clarity. From here on, we will also use the tuples $\mathbf{x} = \{\mathbf{x}_p\}_p$, $\dot{\mathbf{x}} = \{\dot{\mathbf{x}}_p\}_p$, $\mathbf{a} = \{a^j\}_j$, $\dot{\mathbf{a}} = \{\dot{a}^j\}_j$, $\mathbf{b} = \{b^k\}_k$, $\mathbf{e} = \{e^j\}_j$, and $\phi = \{\phi^i\}_i$ to group together the degrees of freedom. Especially it is to be understood that ϕ now refers to the tuple of degrees of freedom, not to the space-continuous electrostatic potential.

Once the above definitions are cleared, one substitutes them to the Vlasov–Maxwell action functional, performs the integrations over phase space, and obtains a finite-dimensional yet time-continuous action functional

$$\begin{aligned} S[\mathbf{x}, \mathbf{a}, \phi] &= \int_{t_i}^{t_f} \frac{\varepsilon_0}{2} e^{j_1} M_{j_1, j_2}^1 e^{j_2} dt \\ &\quad - \int_{t_i}^{t_f} \frac{\mu_0^{-1}}{2} (b^{k_1} + b_{\text{ext}}^{k_1}) M_{k_1, k_2}^2 (b^{k_2} + b_{\text{ext}}^{k_2}) dt \\ &\quad + \sum_p \int_{t_i}^{t_f} q (a^j + a_{\text{ext}}^j) \mathbf{W}_j^1(\mathbf{x}_p) \cdot \dot{\mathbf{x}}_p dt \\ &\quad - \sum_p \int_{t_i}^{t_f} q \phi^i W_i^0(\mathbf{x}_p) dt \\ &\quad + \sum_p \int_{t_i}^{t_f} \frac{1}{2} m |\dot{\mathbf{x}}_p|^2 dt, \end{aligned} \quad (15)$$

where one is to remember the relations $e^j = -\dot{a}^j - \text{grad}_i^j \phi^i$ and $b^k = \text{curl}_j^k a^j$. The constant finite-element mass matrices, related to one-form and two-form element bases, are defined according to

$$\int_{\Omega} \mathbf{W}_{j_1}^1(\mathbf{x}) \cdot \mathbf{W}_{j_2}^1(\mathbf{x}) d\mathbf{x} = M_{j_1, j_2}^1, \quad (16)$$

$$\int_{\Omega} \mathbf{W}_{k_1}^2(\mathbf{x}) \cdot \mathbf{W}_{k_2}^2(\mathbf{x}) d\mathbf{x} = M_{k_1, k_2}^2. \quad (17)$$

From the perspectives of solving the Vlasov–Maxwell system of equations while respecting the Gauss’ law constraints, the electromagnetic gauge invariance turns out

to be a key requirement. Let us first perturb $\mathbf{a} \rightarrow \mathbf{a} + \epsilon \delta \mathbf{a}$ and $\phi \rightarrow \phi + \epsilon \delta \phi$ and differentiate the perturbed action with respect to ϵ at $\epsilon = 0$. This computation provides

$$\begin{aligned} \partial_\epsilon|_{\epsilon=0} S[\mathbf{x}, \mathbf{a} + \epsilon \delta \mathbf{a}, \phi + \epsilon \delta \phi] &= - \int_{t_i}^{t_f} \frac{d}{dt} (\delta a^{j_1} \varepsilon_0 M_{j_1, j_2}^1 e^{j_2}) dt \\ &\quad + \int_{t_i}^{t_f} \delta a^{j_1} \left(\varepsilon_0 M_{j_1, j_2}^1 \dot{e}^{j_2} - \mu_0^{-1} \text{curl}_{j_1}^{k_1} M_{k_1, k_2}^2 (b^{k_2} + b_{\text{ext}}^{k_2}) \right) dt \\ &\quad - \int_{t_i}^{t_f} \delta \phi^{i_1} \varepsilon_0 \text{grad}_{i_1}^{j_1} M_{j_1, j_2}^1 e^{j_2} dt \\ &\quad + \sum_p \int_{t_i}^{t_f} (q \delta a^j \mathbf{W}_j^1(\mathbf{x}_p) \cdot \dot{\mathbf{x}}_p - q \delta \phi^i W_i^0(\mathbf{x}_p)) dt. \end{aligned} \quad (18)$$

Applying the Hamilton’s principle of least action, assuming the perturbations $\delta \mathbf{a}$ and $\delta \phi$ to be arbitrary and to vanish at t_i and t_f , the Euler-Lagrange equations correspond to a discrete Ampère-Maxwell equation

$$\varepsilon_0 M_{j_1, j_2}^1 \dot{e}^{j_2} + J_j = \mu_0^{-1} \text{curl}_{j_1}^{k_1} M_{k_1, k_2}^2 (b^{k_2} + b_{\text{ext}}^{k_2}), \quad (19)$$

and a discrete Gauss’s law for the electric field

$$-\varepsilon_0 \text{grad}_{i_1}^{j_1} M_{j_1, j_2}^1 e^{j_2} = \varrho_i, \quad (20)$$

with current density $J_j = \sum_p q \mathbf{W}_j^1(\mathbf{x}_p) \cdot \dot{\mathbf{x}}_p$ and charge density $\varrho_i = \sum_p q W_i^0(\mathbf{x}_p)$. If, however, we choose the very specific forms for the perturbations

$$\delta a^j = \chi^i \text{grad}_i^j, \quad (21)$$

$$\delta \phi^i = -\dot{\chi}^i, \quad (22)$$

requesting that $\chi^i(t_i) = \chi^i(t_f) = 0$, we observe that the differentiation of the transformed action can now be written as

$$\begin{aligned} \partial_\epsilon|_{\epsilon=0} S[\mathbf{x}, a^j + \epsilon \chi^i \text{grad}_i^j, \phi^i - \epsilon \dot{\chi}^i] &= \int_{t_i}^{t_f} \chi^i \left(\text{grad}_i^j J_j - \dot{\varrho}_i \right) dt. \end{aligned} \quad (23)$$

Because the action also has a strong symmetry with respect to arbitrary χ^i in the sense that

$$S[\mathbf{x}, a^j + \epsilon \chi^i \text{grad}_i^j, \phi^i - \epsilon \dot{\chi}^i] = S[\mathbf{x}, \mathbf{a}, \phi], \quad (24)$$

the differentiation of the transformed action with respect to ϵ has to vanish, providing the finite-dimensional charge conservation law

$$\text{grad}_i^j J_j - \dot{\varrho}_i = 0. \quad (25)$$

The importance of this identity lies in the fact that it eliminates the need to solve the Gauss’ law: Solving for the electric-field $e^j(t)$ in (19) guarantees such evolution for $e^j(t)$ that it automatically satisfies the Gauss’ law (20). It is then a matter of finding a temporal discretization which retains an analog of this property also in the fully discrete case.

III. SUBCYCLING OF PARTICLES WITH AN EXPLICIT FIELD SOLVE

Turning into the details of implementing a subcycling scheme, we first investigate a straightforward modification of existing variational methods. We obtain an algorithm where the particle push is implicit and the field solve explicit, just as in the pioneering work¹. Requesting electromagnetic gauge invariance, the subcycling turns out such that the magnetic field is properly orbit-averaged but the effect of the electric field on the particle orbits is evaluated only once during the subcycling period. Numerical tests then suggest that, if the global time step is too long, the resulting large impulse from a single electric kick might lead to artificial oscillations: we observe the phenomenon in an electrostatically dominated test while it is absent in an electromagnetically dominated test. Enforcing orbit-averaging also for the electric field removes the artificial oscillations but renders the algorithm to no longer be variational. In the section discussing the implicit scheme, we introduce a possible remedy to the issue.

A. Fully variational, gauge-invariant algorithm

The time integral in the action functional is split into intervals $[t_n, t_{n+1}]$, here of equal length Δt , and the total action then comprises of the sum

$$S = \sum_{n=0}^{N-1} S_{n,n+1}. \quad (26)$$

One then assumes some discrete representations for the variable paths in the intervals $t \in [t_n, t_{n+1}]$ and approximates the $S_{n,n+1}$, typically with some quadrature rule. Here, we closely follow the pioneering work¹ but introduce a modification, allowing for subcycling of the particles with \mathcal{V} indicating the number of substeps per global time step Δt .

The discrete action over the time interval $t \in [t_n, t_{n+1}]$ we approximate with the expression

$$\begin{aligned} & S_{n,n+1}[\mathbf{x}_n, \mathbf{x}_{n+1/\mathcal{V}}, \mathbf{x}_{n+2/\mathcal{V}}, \dots, \mathbf{x}_{n+1}, \mathbf{a}_n, \mathbf{a}_{n+1}, \phi_n] \\ &= \Delta t \frac{\varepsilon_0}{2} e_n^{j_1} M_{j_1, j_2}^1 e_n^{j_2} \\ & - \Delta t \frac{\mu_0^{-1}}{2} (b_n^{k_1} + b_{\text{ext}}^{k_1}) M_{k_1 k_2}^2 (b_n^{k_2} + b_{\text{ext}}^{k_2}) \\ & + \sum_p \sum_{\nu=1}^{\mathcal{V}} q (a_{n+1}^j + a_{\text{ext}}^j) \int_0^1 \mathbf{W}_j^1(\mathbf{x}_p^{n,\nu}(\tau)) \cdot \frac{d\mathbf{x}_p^{n,\nu}(\tau)}{d\tau} d\tau \\ & - \sum_p q \phi_n^i W_i^0(\mathbf{x}_{p,n}) \Delta t \\ & + \sum_p \sum_{\nu=1}^{\mathcal{V}} \frac{m}{2} \frac{|\mathbf{x}_{p,n+\nu/\mathcal{V}} - \mathbf{x}_{p,n+(\nu-1)/\mathcal{V}}|^2}{\Delta t/\mathcal{V}}, \end{aligned} \quad (27)$$

where the following abbreviations have been introduced

$$b_n^k = a_n^j \text{curl}_j^k, \quad (28)$$

$$e_n^j = -(a_{n+1}^j - a_n^j)/\Delta t - \phi_n^i \text{grad}_i^j, \quad (29)$$

and $\mathbf{x}_p^{n,\nu}(\tau)$ is a straight trajectory connecting the substeps $(\nu-1)$ and ν linked to a global step n and defined according to

$$\mathbf{x}_p^{n,\nu}(\tau) = (1-\tau)\mathbf{x}_{p,n+(\nu-1)/\mathcal{V}} + \tau\mathbf{x}_{p,n+\nu/\mathcal{V}}. \quad (30)$$

The discrete Euler–Lagrange conditions are derived by perturbing the variables, assuming the perturbations to vanish at the end points in time, and looking for an extrema point of the discrete action. With respect to the perturbations $\mathbf{a}_n \rightarrow \mathbf{a}_n + \varepsilon\delta\mathbf{a}_n$, this leads to the equation

$$\begin{aligned} & \partial_\varepsilon|_{\varepsilon=0} S_{n,n+1}[\mathbf{a}_n + \varepsilon\delta\mathbf{a}_n] \\ & + \partial_\varepsilon|_{\varepsilon=0} S_{n-1,n}[\mathbf{a}_n + \varepsilon\delta\mathbf{a}_n] = 0, \end{aligned} \quad (31)$$

and, when written explicitly, provides the discrete Ampère–Maxwell equation

$$\varepsilon_0 M_{j,j_2}^1 \frac{e_{n+1}^{j_2} - e_n^{j_2}}{\Delta t} + J_j^{n,n+1} = \mu_0^{-1} \text{curl}_j^k M_{k,k_2}^2 (b_{n+1}^{k_2} + b_{\text{ext}}^{k_2}), \quad (32)$$

with a discrete current density defined according to

$$J_j^{n,n+1} = \sum_p \sum_{\nu=1}^{\mathcal{V}} q \int_0^1 \mathbf{W}_j^1(\mathbf{x}_p^{n,\nu}(\tau)) \cdot \frac{d\mathbf{x}_p^{n,\nu}(\tau)}{d\tau} \frac{d\tau}{\Delta t}. \quad (33)$$

With respect to perturbations $\phi_n \rightarrow \phi_n + \varepsilon\delta\phi_n$, the variation of the action leads to

$$\partial_\varepsilon|_{\varepsilon=0} S_{n,n+1}[\phi_n + \varepsilon\delta\phi_n] = 0, \quad (34)$$

which, when written explicitly, corresponds to the discrete Gauss' law

$$\varrho_i^n = -\varepsilon_0 \text{grad}_i^j M_{j,j_2}^1 e_n^{j_2}, \quad (35)$$

with the discrete charge density being defined according to

$$\varrho_i^n = \sum_p q W_i^0(\mathbf{x}_{p,n}). \quad (36)$$

Perturbing the particles' spatial positions $\mathbf{x}_n \rightarrow \mathbf{x}_n + \varepsilon\delta\mathbf{x}_n$ provides

$$\begin{aligned} & \partial_\varepsilon|_{\varepsilon=0} S_{n,n+1}[\mathbf{x}_n + \varepsilon\delta\mathbf{x}_n] \\ & + \partial_\varepsilon|_{\varepsilon=0} S_{n-1,n}[\mathbf{x}_n + \varepsilon\delta\mathbf{x}_n] = 0 \end{aligned} \quad (37)$$

while perturbing $\mathbf{x}_{n+\nu/\mathcal{V}} \rightarrow \mathbf{x}_{n+\nu/\mathcal{V}} + \varepsilon\delta\mathbf{x}_{n+\nu/\mathcal{V}}$ provides

$$\partial_\varepsilon|_{\varepsilon=0} S_{n,n+1}[\mathbf{x}_{n+\nu/\mathcal{V}} + \varepsilon\delta\mathbf{x}_{n+\nu/\mathcal{V}}] = 0, \quad (38)$$

for each $n = 0, \dots, N-1$ and $\nu = 1, \dots, \mathcal{V}-1$. Written explicitly, these correspond to the equations for the indices n

$$\begin{aligned}
& m \frac{\mathbf{x}_{p,n+1/\mathcal{V}} - 2\mathbf{x}_{p,n} + \mathbf{x}_{p,n-1/\mathcal{V}}}{(\Delta t/\mathcal{V})^2} \\
&= q \frac{\mathbf{x}_{n+1/\mathcal{V}} - \mathbf{x}_{p,n}}{\Delta t/\mathcal{V}} \\
&\quad \times \int_0^1 (1-\tau)(b_{n+1}^k + b_{\text{ext}}^k) \mathbf{W}_k^2(\mathbf{x}_p^{n,1}(\tau)) d\tau \\
&+ q \frac{\mathbf{x}_{p,n} - \mathbf{x}_{p,n-1/\mathcal{V}}}{\Delta t/\mathcal{V}} \\
&\quad \times \int_0^1 \tau(b_n^k + b_{\text{ext}}^k) \mathbf{W}_k^2(\mathbf{x}_p^{n,0}(\tau)) d\tau \\
&+ q\mathcal{V}e_n^j \mathbf{W}_j^1(\mathbf{x}_{p,n}). \tag{39}
\end{aligned}$$

and for the indices ν

$$\begin{aligned}
& m \frac{\mathbf{x}_{p,n+(\nu+1)/\mathcal{V}} - 2\mathbf{x}_{p,n+\nu/\mathcal{V}} + \mathbf{x}_{p,n+(\nu-1)/\mathcal{V}}}{(\Delta t/\mathcal{V})^2} \\
&= q \frac{\mathbf{x}_{n+(\nu+1)/\mathcal{V}} - \mathbf{x}_{p,n+\nu/\mathcal{V}}}{\Delta t/\mathcal{V}} \\
&\quad \times \int_0^1 (1-\tau)(b_{n+1}^k + b_{\text{ext}}^k) \mathbf{W}_k^2(\mathbf{x}_p^{n,\nu+1}(\tau)) d\tau \\
&+ q \frac{\mathbf{x}_{p,n+\nu/\mathcal{V}} - \mathbf{x}_{p,n+(\nu-1)/\mathcal{V}}}{\Delta t/\mathcal{V}} \\
&\quad \times \int_0^1 \tau(b_{n+1}^k + b_{\text{ext}}^k) \mathbf{W}_k^2(\mathbf{x}_p^{n,\nu}(\tau)) d\tau. \tag{40}
\end{aligned}$$

Note that the electric-field impulse is evaluated only for steps with index n , not for the ν .

The equations (32), (35), (39), and (40) are completed by the discrete Faraday equation that is a direct consequence of the definitions for $\mathbf{e}_n, \mathbf{b}_n$, namely

$$\frac{b_n^k - b_{n-1}^k}{\Delta t} = -\text{curl}_j^k e_{n-1}^j. \tag{41}$$

The electromagnetic gauge invariance and the discrete charge conservation law are verified in the following manner. Let

$$a_n^j \rightarrow a_n^j + \chi_n^i \text{grad}_i^j, \tag{42}$$

$$\phi_n^i \rightarrow \phi_n^i - \frac{\chi_{n+1}^i - \chi_n^i}{\Delta t}, \tag{43}$$

and the total discrete action (27) will satisfy the strong symmetry condition

$$\begin{aligned}
& \sum_{n=0}^{N-1} S_{n,n+1} [a_n^j + \chi_n^i \text{grad}_i^j, a_{n+1}^j + \chi_{n+1}^i \text{grad}_i^j, \\
&\quad \phi_n^i - (\chi_{n+1}^i - \chi_n^i)/\Delta t] \\
&= \sum_{n=0}^{N-1} S_{n,n+1} [\mathbf{a}_n, \mathbf{a}_{n+1}, \phi_n] \\
&+ \sum_p e_p [\chi_N^i W_i^0(\mathbf{x}_{p,N}) - \chi_0^i W_i^0(\mathbf{x}_{p,0})]. \tag{44}
\end{aligned}$$

Differentiating with respect to χ_n at any n such that $n \neq 0$ and $n \neq N$, the right side vanishes identically as it is independent of χ_n , and one finds the discrete charge conservation law

$$\text{grad}_i^j J_j^{n-1,n} - \frac{\varrho_i^n - \varrho_i^{n-1}}{\Delta t} = 0. \tag{45}$$

The significance of this equation is that, if we assume the Gauss' law (35) to hold for $n-1$, the charge conservation and the Ampère equation (32) then imply

$$\varrho_i^n = \varrho_i^{n-1} + \Delta t \text{grad}_i^j J_j^{n-1,n} = -\varepsilon_0 \text{grad}_i^j M_{j,j_2}^1 e_n^{j_2}, \tag{46}$$

meaning that the Gauss' law is automatically satisfied, if it is satisfied initially.

Together the discrete equations provide means of advancing the degrees of freedom $\mathbf{x}_n, \mathbf{e}_n$, and \mathbf{b}_n in time according to the following strategy

0. Given \mathbf{x}_0 , initialize \mathbf{e}_0 with the Gauss's law (35) and approximate $\mathbf{x}_{-1/\mathcal{V}}$ using \mathbf{v}_0
1. Given $\mathbf{e}_n, \mathbf{b}_n$, compute \mathbf{b}_{n+1} from the Faraday equation (41)
2. Given $(\mathbf{e}_n, \mathbf{b}_n, \mathbf{b}_{n+1})$ and $(\mathbf{x}_{n-1/\mathcal{V}}, \mathbf{x}_n)$, push markers with (39) to obtain $\mathbf{x}_{n+1/\mathcal{V}}$
3. Given $\mathbf{x}_n, \mathbf{x}_{n+1/\mathcal{V}}$ and $\mathbf{b}_n, \mathbf{b}_{n+1}$, push markers to $\mathbf{x}_{n+2/\mathcal{V}}, \dots, \mathbf{x}_{n+1}$ with (40) and accumulate $J_j^{n,n+1}$ according to (33)
4. Given $\mathbf{e}_n, \mathbf{b}_{n+1}$ and the recorded value for $J_j^{n,n+1}$, invert the Ampère-Maxwell equation (32) for \mathbf{e}_{n+1}
5. Repeat the steps 1-4 indefinitely

B. Numerical tests

We have implemented the subcycling method within the GEMPIC code in the library `SeLaLib`²³. The code is based on compatible spline-finite-element bases as described in⁹. The major building blocks of our algorithm are very similar to the Hamiltonian splitting used in⁹, which we shall use for benchmarking purposes. However, the new subcycling scheme does not build upon a splitting of the kinetic energy into the three components and contains a non-linearity in equations (39) and (40). This non-linearity, however, only couples the three components of the three positions of each particle. This non-linear step can efficiently be solved by a first guess obtained by extrapolation from the old values, followed by one or more updates according to Newton's method. For this, an analytic formula for the derivative matrix can be found and evaluated numerically in the implementation.

1. An electrostatically dominated test case

As a first example of a simulation with strong background magnetic field, we consider a reduced, 1D-2V-dimensional phase space and an initial distribution function of

$$f(x, v_1, v_2) = \frac{1 + 0.1 \cos(0.5x)}{2\pi} \exp\left(-\frac{v_1^2 + v_2^2}{2}\right), \quad (47)$$

set up in a background magnetic field of $B_3(x, 0) = 2\pi 10$. We run the variational subcycling and the Hamiltonian splitting algorithms with 32 grid points and 160,000 particles until time 30. In this case, the spatial resolution is given by $\Delta x = 4\pi/32$. Since we split the curl-part in Faraday's and Ampère's law, we get a stability limit of $\Delta t < \Delta x \sqrt{17/42} \approx 0.2498$ (cf.²² (Appendix A2)).

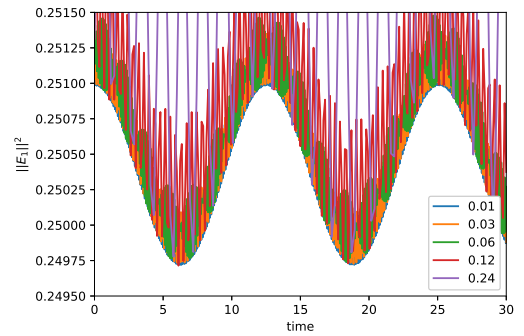
For our choice of the magnetic field, the gyro-period is 0.1. For a time step of $\Delta t = 0.01$ this time scale is resolved well and good results can be obtained even without subcycling. We then increase the global time step to 0.03, 0.06, 0.12, and 0.24. For the Hamiltonian splitting from⁹, the simulation runs only stable for $\Delta t = 0.01, 0.03$ and already in the latter case the quality of the result is degraded (see Figure 1b). Figure 1a shows the results of the simulation with our variational subcycling scheme with one step for $\Delta t = 0.01$ and two substeps for all other global time steps. For the nonlinear iteration, we compute the initial guess followed by 2-3 Newton iterations on average to reach an accuracy of 10^{-10} for the individual particle positions. We see that the simulations run stable until the stability limit due to the split in the curl-part of Maxwell's equation. On the other hand, the results show quite high oscillations which we believe to be linked to the way the effect of electric field impulse is evaluated on the particle orbits. Table 1a shows the maximum error in Gauss' law over the whole simulation, which confirms the conservation properties of the subcycling algorithm, while Table 1b shows the error in the conservation of energy, which naturally grows with increasing of the global time step.

Increasing the number of subcycles to two (as done in the reported experiments) results in a slight improvement of the results. For more than two subcycles, the quality of the results decreases again in the sense that the artificial oscillations begin to grow. This indicates that a subcycling algorithm that does not include orbit averaging of the electric field does not work well with strong electric fields.

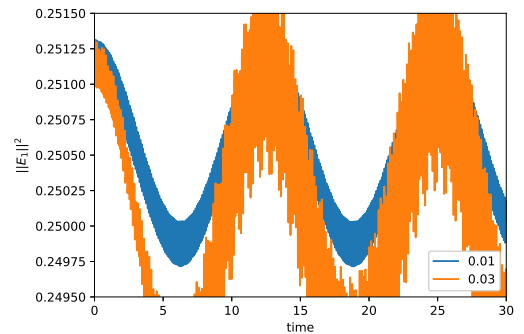
2. An electromagnetic test case

As a second example, we look at an electromagnetically dominated test case with initial distribution

$$f(x, v_1, v_2) = \frac{1 + 0.1 \cos(kx)}{2\pi\sigma_1\sigma_2} \exp\left(-\left(\frac{v_1^2}{2\sigma_1^2} + \frac{v_2^2}{2\sigma_2^2}\right)\right), \quad (48)$$



(a) Variational subcycling.



(b) Hamiltonian splitting.

FIG. 1: Electrostatically dominated test case: Time evolution of $\|E_1\|^2$ for the different integrators with various time steps (given in the legends) with $B(x, 0) = 2\pi 10$.

Δt	Ham. splitting	Var. subcycl.
0.01	$1.41 \cdot 10^{-13}$	$1.39 \cdot 10^{-13}$
0.03	$1.40 \cdot 10^{-13}$	$1.38 \cdot 10^{-13}$
0.06	—	$1.39 \cdot 10^{-13}$
0.12	—	$1.39 \cdot 10^{-13}$
0.24	—	$1.40 \cdot 10^{-13}$

(a) Conservation of Gauss' law

Δt	Ham. splitting	Var. subcycl.
0.01	$6.76 \cdot 10^{-2}$	$5.16 \cdot 10^{-5}$
0.03	$4.43 \cdot 10^1$	$1.56 \cdot 10^{-4}$
0.06	—	$4.08 \cdot 10^{-4}$
0.12	—	$1.04 \cdot 10^{-3}$
0.24	—	$3.39 \cdot 10^{-3}$

(b) Conservation of energy

TABLE I: Electrostatic test case: Conservation laws for various propagators and time steps.

and initial magnetic field $B_0(x) = \beta_1 + \beta_2 \cos(kx)$ on the domain $[0, \frac{2\pi}{k})$. We choose the parameters to be $k = 1.25$, $\sigma_1 = \sqrt{2} \cdot 0.01$, $\sigma_2 = \sqrt{12}\sigma_1$, $\beta_1 = 20\pi$, $\beta_2 = 0.001$. This test case is electromagnetic and a variation of the Weibel instability with a strong background field. The example is a variation of the test problem proposed in²⁴.

We run a simulation until time 20 with 32 grid points, 100,000 particles, and spline basis functions of degree 3. The stability limit due to the splitting of the Maxwell's equation is at $\Delta t < (2\pi)/(1.25 \times 32)\sqrt{17/42} \approx 0.09994$ in this case.

Figures 2a and 2b show the electric energy for simulations with variational subcycling and Hamiltonian splitting, respectively, for various time steps. In this test case, both the Hamiltonian splitting and the variational subcycling scheme yield stable results until the stability limit of the Maxwell part is reached. However, the quality of the results is considerably better with the variational subcycling scheme for the larger time steps of 0.06 and 0.09. We report here the results with 1 ($\Delta t = 0.01$), 2 ($\Delta t = 0.03$), 4 ($\Delta t = 0.06, 0.09$) substeps per one global time step. We note that we did not further increase the number of subcycles when increasing the time step from 0.06 to 0.09, since no improvement in accuracy was observed beyond the 4 subcycles. The number of Newton updates needed to reach the convergence down to a tolerance of 10^{-10} is between 1 and 2 on average in all four simulations. Table IIa shows the maximum error in Gauss' law over the whole simulation, which again confirms the conservation properties of the variational subcycling algorithm. Table IIb shows the error in the conservation of energy, which grows with increasing of the global time step.

Δt	Ham. splitting	Var. subcycl.
0.01	$1.52 \cdot 10^{-14}$	$1.50 \cdot 10^{-14}$
0.03	$1.50 \cdot 10^{-14}$	$1.50 \cdot 10^{-14}$
0.06	$1.53 \cdot 10^{-14}$	$1.51 \cdot 10^{-14}$
0.09	$1.48 \cdot 10^{-14}$	$1.48 \cdot 10^{-14}$

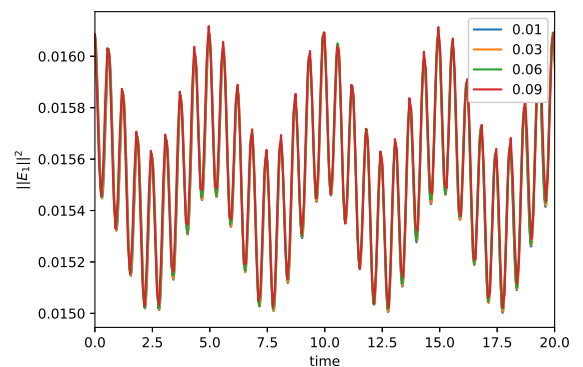
(a) Conservation of Gauss' law

Δt	Ham. splitting	Var. subcycl.
0.01	$1.40 \cdot 10^{-5}$	$8.71 \cdot 10^{-6}$
0.03	$1.26 \cdot 10^{-4}$	$2.79 \cdot 10^{-5}$
0.06	$4.99 \cdot 10^{-4}$	$6.17 \cdot 10^{-5}$
0.09	$1.11 \cdot 10^{-3}$	$1.00 \cdot 10^{-4}$

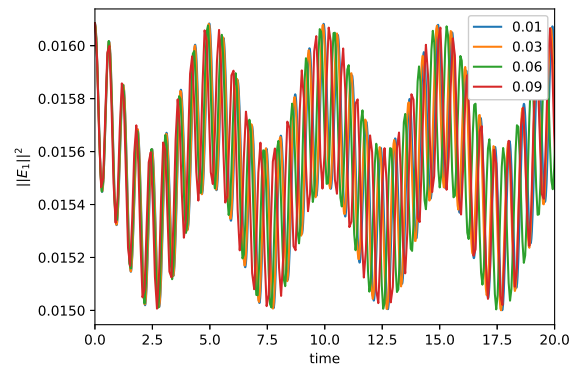
(b) Conservation of energy

TABLE II: Electromagnetic test case: Conservation laws for different propagators and time steps.

Notice that in this electromagnetic case, we do not observe any spurious oscillations when introducing subcycling of particle orbits. This is likely due to the impulse from the electric-field push remaining small enough, even when it is evaluated only once per subcycle. This is supported by noticing that the electric energy in this test case is an order of magnitude lower than in the electrostatically dominated case.



(a) Variational subcycling.



(b) Hamiltonian splitting.

FIG. 2: Electromagnetically dominated test case: Time evolution of $\|E_1\|^2$ for the different integrators with various time steps (given in the legends) with $B(x, 0) = 10 + 0.001 \cos(kx)$.

C. Enforcing orbit averaging

To investigate whether the root cause for the possible numerical oscillations is indeed in the way the electric field is evaluated in particle orbits, we will now enforce orbit averaging also for the electric-field contribution. For the indices n , we will use the following modified particle push

$$\begin{aligned}
 & m \frac{\mathbf{x}_{p,n+1/\nu} - 2\mathbf{x}_{p,n} + \mathbf{x}_{p,n-1/\nu}}{(\Delta t/\nu)^2} \\
 &= q \frac{\mathbf{x}_{n+1/\nu} - \mathbf{x}_{p,n}}{\Delta t/\nu} \\
 &\quad \times \int_0^1 (1-\tau)(b_{n+1}^k + b_{\text{ext}}^k) \mathbf{W}_k^2(\mathbf{x}_p^{n,1}(\tau)) d\tau \\
 &+ q \frac{\mathbf{x}_{p,n} - \mathbf{x}_{p,n-1/\nu}}{\Delta t/\nu} \\
 &\quad \times \int_0^1 \tau(b_n^k + b_{\text{ext}}^k) \mathbf{W}_k^2(\mathbf{x}_p^{n,0}(\tau)) d\tau \\
 &+ q e_n^j \mathbf{W}_j^1(\mathbf{x}_{p,n}), \tag{49}
 \end{aligned}$$

and similarly for the indices ν

$$\begin{aligned}
& m \frac{\mathbf{x}_{p,n+(\nu+1)/\nu} - 2\mathbf{x}_{p,n+\nu/\nu} + \mathbf{x}_{p,n+(\nu-1)/\nu}}{(\Delta t/\nu)^2} \\
&= q \frac{\mathbf{x}_{n+(\nu+1)/\nu} - \mathbf{x}_{p,n+\nu/\nu}}{\Delta t/\nu} \\
&\quad \times \int_0^1 (1-\tau)(b_{n+1}^k + b_{\text{ext}}^k) \mathbf{W}_k^2(\mathbf{x}_p^{n,\nu+1}(\tau)) d\tau \\
&+ q \frac{\mathbf{x}_{p,n+\nu/\nu} - \mathbf{x}_{p,n+(\nu-1)/\nu}}{\Delta t/\nu} \\
&\quad \times \int_0^1 \tau(b_{n+1}^k + b_{\text{ext}}^k) \mathbf{W}_k^2(\mathbf{x}_p^{n,\nu}(\tau)) d\tau \\
&+ q e_n^j \mathbf{W}_j^1(\mathbf{x}_{p,n+\nu/\nu}). \tag{50}
\end{aligned}$$

We stress that this particle push is not derived from an action principle and is not expected to provide bounded long-time energy behavior like the variational schemes, nor to conserve the multisymplectic two-form. For the field equations, we use the Ampère and Gauss' law as described previously for they satisfy a charge conservation law regardless of how the particle orbits are sampled.

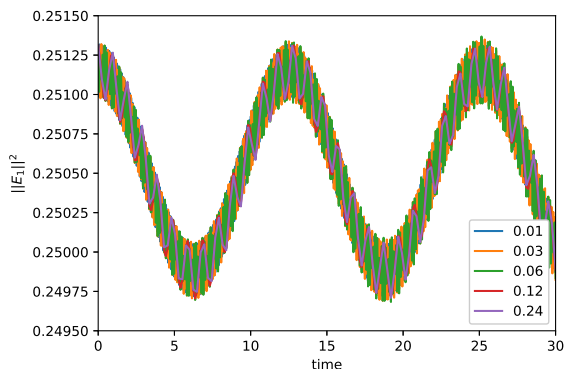


FIG. 3: Electrostatically dominated test case: Time evolution of $\|E_1\|^2$ for the subcycling algorithm with enforced electric-field orbit-averaging for various time steps (given in the legends).

We then repeated the numerical tests from the previous section using the above particle equations. For the electrostatically dominated test case, Figure 3 shows the evolution of the first component of the electric energy as a function of time with the new algorithm and the number of subcycles increased to 4 ($\Delta t = 0.06$), 8 ($\Delta t = 0.12$), and 16 ($\Delta t = 0.24$). We observe that the artificial oscillations are indeed gone. The behaviour of the solution remains better even if the global step size is increased beyond the cyclotron period, which is our ultimate goal. In the electromagnetically dominated test case, we do not see further improvements from the original algorithm for it worked well.

IV. AN IMPLICIT SCHEME WITH FULL ORBIT AVERAGING AND ELECTROMAGNETIC GAUGE INVARIANCE

To find a variational scheme that would succeed in fully orbit averaging the particle trajectories, we suggest a temporal discretization that appears to lead to a fully implicit scheme. Essentially, we have learned that the key likely is in handling the interaction term in the action integral in a manner that properly allows one to perform integration by parts in time, instead of the summation-by-parts trick that works nicely without subcycling and apparently with certain limitations together with subcycling as described in Sec. III. It remains to be seen whether an explicit field-solve strategy, succeeding in both proper orbit-averaging and electromagnetic gauge-invariance, is possible. We also introduce arbitrary time steps for it might be useful in near future for adaptive temporal integration.

A. Polyline particle trajectories

We will now assume that the particle trajectories form a polyline between different time instances and shall respect this assumption in the discretization. We partition the interval $[t_i, t_f]$ into multiple arbitrary intervals $t_i = t_0 < t_1 < \dots < t_{m-1} < t_m < t_{m+1} < \dots < t_f$ and during each interval, the particle trajectory is expressed as

$$\mathbf{x}_p^{m,m+1}(t) = \mathbf{x}_{p,m} + \frac{t - t_m}{t_{m+1} - t_m} (\mathbf{x}_{p,m+1} - \mathbf{x}_{p,m}), \tag{51}$$

$$\dot{\mathbf{x}}_p^{m,m+1}(t) = \frac{\mathbf{x}_{p,m+1} - \mathbf{x}_{p,m}}{t_{m+1} - t_m}, \tag{52}$$

making sure that the time derivative is consistent with the trajectory. Substituting these expressions into the action, we find the following particle-relevant contribution over the interval $[t_m, t_{m+1}]$

$$\begin{aligned}
& S_{m,m+1}^p[\mathbf{a}(t), \phi(t), \mathfrak{x}_m, \mathfrak{x}_{m+1}] \\
&= q \int_{t_m}^{t_{m+1}} (a^j(t) + a_{\text{ext}}^j) \mathbf{W}_j^1(\mathbf{x}_p^{m,m+1}(t)) \cdot \dot{\mathbf{x}}_p^{m,m+1}(t) dt \\
&\quad - q \int_{t_m}^{t_{m+1}} \phi^i(t) W_i^0(\mathbf{x}_p^{m,m+1}(t)) dt \\
&\quad + \frac{1}{2} m \int_{t_m}^{t_{m+1}} |\dot{\mathbf{x}}_p^{m,m+1}|^2 dt. \tag{53}
\end{aligned}$$

Perturbing the particle polylines into $\mathfrak{x}_m + \epsilon \delta \mathfrak{x}_m$ and minimizing the action with respect to the variations in the particle positions, we obtain the following discrete Euler-Lagrange condition for each particle

$$\begin{aligned}
& \partial_\epsilon|_{\epsilon=0} S_{m,m+1}^p[\mathbf{x}_{p,m} + \epsilon \delta \mathbf{x}_{p,m}] \\
&+ \partial_\epsilon|_{\epsilon=0} S_{m-1,m}^p[\mathbf{x}_{p,m} + \epsilon \delta \mathbf{x}_{p,m}] = 0. \tag{54}
\end{aligned}$$

Written explicitly, this corresponds to the following discrete Euler–Lagrange condition

$$\begin{aligned}
& m \frac{\mathbf{x}_{p,m+1} - \mathbf{x}_{p,m}}{t_{m+1} - t_m} - m \frac{\mathbf{x}_{p,m} - \mathbf{x}_{p,m-1}}{t_m - t_{m-1}} \\
&= q \frac{\mathbf{x}_{p,m+1} - \mathbf{x}_{p,m}}{t_{m+1} - t_m} \\
&\quad \times \int_{t_m}^{t_{m+1}} \frac{t_{m+1} - t}{t_{m+1} - t_m} (b^k(t) + b_{\text{ext}}^k) \mathbf{W}_k^2(\mathbf{x}_p^{m,m+1}(t)) dt \\
&+ q \frac{\mathbf{x}_{p,m} - \mathbf{x}_{p,m-1}}{t_m - t_{m-1}} \\
&\quad \times \int_{t_{m-1}}^{t_m} \frac{t - t_{m-1}}{t_m - t_{m-1}} (b^k(t) + b_{\text{ext}}^k) \mathbf{W}_k^2(\mathbf{x}_p^{m-1,m}(t)) dt \\
&+ q \int_{t_{m-1}}^{t_m} \frac{t - t_{m-1}}{t_m - t_{m-1}} e^j(t) \mathbf{W}_j^1(\mathbf{x}_p^{m-1,m}(t)) dt \\
&+ q \int_{t_m}^{t_{m+1}} \frac{t_{m+1} - t}{t_{m+1} - t_m} e^j(t) \mathbf{W}_j^1(\mathbf{x}_p^{m,m+1}(t)) dt, \quad (55)
\end{aligned}$$

where we have associated $e^j(t) = -\dot{a}^j(t) - \phi^i(t) \text{grad}_i^j$.

In deriving the expression (55), it was necessary to request time-continuity for $a^j(t)$ but not for $\phi^i(t)$. Hence we can imagine a piece-wise time-constant electric field $e^j(t) = -\dot{a}^j(t) - \text{grad}_i^j \phi^i(t)$. The magnetic field $b^k(t)$ appearing in the particle equation, however, has to be at least piece-wise linear in time for it needs to be compatible with the requirement of at least piecewise linear $a^j(t)$ in the interaction part of the action.

B. Polyline $a(t)$ and piece-wise constant $\phi(t)$

Next we partition the interval $[t_i, t_f]$ according to $t_i = t_0 < t_1 < \dots < t_{n-1} < t_n < t_{n+1} < \dots < t_f$, again with arbitrary intervals. During each interval $[t_n, t_{n+1}]$ we assume the following behaviour for the electromagnetic degrees of freedom

$$a_{n,n+1}^j(t) = a_n^j + \frac{t - t_n}{t_{n+1} - t_n} (a_{n+1}^j - a_n^j), \quad (56)$$

$$\phi_{n,n+1}^i(t) = \phi_n^i, \quad (57)$$

which implies that we can define the electric and magnetic field during the interval directly via the relations

$$b_{n,n+1}^k(t) = a_{n,n+1}^j(t) \text{curl}_j^k \equiv b_n^k + \frac{t - t_n}{t_{n+1} - t_n} (b_{n+1}^k - b_n^k), \quad (58)$$

$$e_{n,n+1}^j(t) = -\frac{a_{n+1}^j - a_n^j}{t_{n+1} - t_n} - \phi_n^i \text{grad}_i^j \equiv e_n^j. \quad (59)$$

The above discretizations satisfy the requirements for the magnetic field and potential to be at least time-continuous and the electric field at least piece-wise constant, thus being compatible with (55). The discretization also implies a form for the discrete Faraday law

$$\frac{b_{n+1}^k - b_n^k}{t_{n+1} - t_n} = -e_n^j \text{curl}_j^k. \quad (60)$$

Substituting these expressions into the action, we find the following electromagnetic-relevant contribution over the interval $[t_n, t_{n+1}]$

$$\begin{aligned}
& S_{n,n+1}^{\text{EM}}[\mathbf{a}_n, \mathbf{a}_{n+1}, \phi_n, \mathbf{x}(t)] \\
&= \frac{\varepsilon_0}{2} e_n^{j_1} M_{j_1, j_2}^1 e_n^{j_2} (t_{n+1} - t_n) \\
&\quad - \frac{\mu_0^{-1}}{2} \int_{t_n}^{t_{n+1}} (b_{n,n+1}^{k_1}(t) + b_{\text{ext}}^{k_1}) M_{k_1 k_2}^2 (b_{n,n+1}^{k_2}(t) + b_{\text{ext}}^{k_2}) dt \\
&\quad + \sum_p \int_{t_n}^{t_{n+1}} q (a_{n,n+1}^j(t) + a_{\text{ext}}^j) \mathbf{W}_j^1(\mathbf{x}_p(t)) \cdot \dot{\mathbf{x}}_p(t) dt \\
&\quad - \sum_p \int_{t_n}^{t_{n+1}} q \phi_n^i W_i^0(\mathbf{x}_p(t)) dt. \quad (61)
\end{aligned}$$

Next we perturb the degrees of freedom for the vector potential into $\mathbf{a}_n + \epsilon \delta \mathbf{a}_n$ and minimize the action with respect to the variations $\delta \mathbf{a}_n$. This provides the discrete Euler–Lagrange equation

$$\partial_{\epsilon}|_{\epsilon=0} S_{n,n+1}^{\text{EM}}[\mathbf{a}_n + \epsilon \delta \mathbf{a}_n] + \partial_{\epsilon}|_{\epsilon=0} S_{n-1,n}^{\text{EM}}[\mathbf{a}_n + \epsilon \delta \mathbf{a}_n] = 0, \quad (62)$$

and explicitly it provides the following discrete Ampère equation

$$\begin{aligned}
& \varepsilon_0 M_{j_1, j_2}^1 (e_n^{j_2} - e_{n-1}^{j_2}) + J_{j_+}^{n,n+1} + J_{j_-}^{n-1,n} \\
&= \mu_0^{-1} \text{curl}_{j_1}^{k_1} M_{k_1 k_2}^2 \left(\frac{1}{6} b_{n+1}^{k_2} + \frac{1}{3} b_n^{k_2} + \frac{1}{2} b_{\text{ext}}^{k_2} \right) (t_{n+1} - t_n) \\
&\quad + \mu_0^{-1} \text{curl}_{j_1}^{k_1} M_{k_1 k_2}^2 \left(\frac{1}{3} b_n^{k_2} + \frac{1}{6} b_{n-1}^{k_2} + \frac{1}{2} b_{\text{ext}}^{k_2} \right) (t_n - t_{n-1}), \quad (63)
\end{aligned}$$

where the discrete current densities are defined via the relations

$$J_{j_+}^{n,n+1} = q \sum_p \int_{t_n}^{t_{n+1}} \frac{t_{n+1} - t}{t_{n+1} - t_n} \mathbf{W}_{j_1}^1(\mathbf{x}_p(t)) \cdot \dot{\mathbf{x}}_p(t) dt, \quad (64)$$

$$J_{j_-}^{n,n+1} = q \sum_p \int_{t_n}^{t_{n+1}} \frac{t - t_n}{t_{n+1} - t_n} \mathbf{W}_{j_1}^1(\mathbf{x}_p(t)) \cdot \dot{\mathbf{x}}_p(t) dt. \quad (65)$$

Note that in deriving the expression (63), it is enough to require continuity from $\mathbf{x}_p(t)$, while the corresponding $\dot{\mathbf{x}}_p(t)$ can be piece-wise constant. Hence this Ampère equation and the equation for the particle motion (55) are fully compatible with each other. One only has to account for the fact that the instances t_n and t_m do not necessarily coincide.

Finally, perturbing the degrees for the scalar potential to $\phi_n + \epsilon \delta \phi_n$ and extremizing the action with respect to arbitrary variations $\delta \phi_n$ according to

$$\partial_{\epsilon}|_{\epsilon=0} S_{n,n+1}^{\text{EM}}[\phi_n + \epsilon \delta \phi_n] = 0 \quad (66)$$

provides the discrete Gauss' law

$$\varrho_i^{n,n+1} = -\varepsilon_0 \text{grad}_i^j M_{j, j_2}^1 e_n^{j_2}, \quad (67)$$

where the discrete charge density is defined as

$$\varrho_i^{n,n+1} = q \sum_p \int_{t_n}^{t_{n+1}} W_i^0(\mathbf{x}_p(t)) \frac{dt}{t_{n+1} - t_n}. \quad (68)$$

C. Gauge invariance and the charge-conservation law

To demonstrate that the Gauss' law (67) serves only as an initial condition and that it is enough to advance the electric field degrees of freedom via the discrete Ampère equation (63), we start from the electromagnetic gauge invariance.

We define a gauge transformation with a function

$$\chi_{n,n+1}^i(t) = \chi_n^i + \frac{t - t_n}{t_{n+1} - t_n} (\chi_{n+1}^i - \chi_n^i), \quad (69)$$

and change the discrete vector and scalar potentials according to

$$a_{n,n+1}^j(t) \rightarrow a_{n,n+1}^j(t) + \chi_{n,n+1}^i(t) \text{grad}_i^j, \quad (70)$$

$$\phi_{n,n+1}^i(t) \rightarrow \phi_{n,n+1}^i(t) - \dot{\chi}_{n,n+1}^i(t). \quad (71)$$

The discrete electric and magnetic field are trivially unchanged under these substitutions and the relevant part of the action then satisfies

$$\begin{aligned} & \sum_{n=0}^{N-1} S_{n,n+1}^{\text{EM}} [a_n^j + \text{grad}_i^j \chi_n^i, a_{n+1} + \text{grad}_i^j \chi_{n+1}^i, \\ & \quad \phi_n - (\chi_{n+1}^i - \chi_n^i)/(t_{n+1} - t_n)] \\ &= \sum_{n=0}^{N-1} S_{n,n+1}^{\text{EM}} [a_n^j, a_{n+1}, \phi_n] \\ &+ q \sum_p [\chi_N^i W_i^0(\mathbf{x}_p(t_f)) - \chi_0^i W_i^0(\mathbf{x}_p(t_i))]. \end{aligned} \quad (72)$$

Proceeding as previously, i.e., differentiating the above relation with respect to χ_n^i for arbitrary $n \in \{1, \dots, N-1\}$, provides the discrete charge conservation law

$$\text{grad}_i^j \left(J_{j+}^{n,n+1} + J_{j-}^{n-1,n} \right) - \left(\varrho_i^{n,n+1} - \varrho_i^{n-1,n} \right) = 0, \quad (73)$$

where the current and charge densities are as defined in the equations (64), (65), and (68).

Assuming the discrete Gauss' law (67) to hold for $n-1$, it is then a straightforward task to use the Ampère equation (63) together with the charge conservation law (73) to obtain

$$\begin{aligned} \varrho_i^{n,n+1} &= \varrho_i^{n-1,n} - \text{grad}_i^j \left(J_{j+}^{n,n+1} + J_{j-}^{n-1,n} \right) \\ &= -\varepsilon_0 \text{grad}_i^j M_{j,j_2}^1 e_n^{j_2}. \end{aligned} \quad (74)$$

This means that, if the Gauss' law holds initially, it will be satisfied for all times when we solve the electric field from the Ampère equation. This result is fully analogous with the one we obtained for the algorithm with an explicit field solve in Sec. III.

D. Solver strategy and equal-step sequencing

Next we propose one possible strategy to implement the implicit scheme as described above, using equal step sizes for all but the first global step and fixed-point iteration for the nonlinear solves. Letting \mathcal{V} denote the number of particle subcycling steps per one global time step Δt , we define for $n=1, m=1$

$$t_1 = t_0 + \Delta t/\mathcal{V}, \quad (75)$$

while for $n > 1, m > 1$ we define

$$t_{n+1} = t_n + \Delta t, \quad (76)$$

$$t_{m+1} = t_m + \Delta t/\mathcal{V}. \quad (77)$$

Introducing the index ν as in the explicit section, one could then interpret the time instances t_m to correspond to $t_{n+\nu/\mathcal{V}} = t_n + \nu/\mathcal{V} \Delta t$, with $n = \lfloor (m + (\mathcal{V}-1))/\mathcal{V} \rfloor$, $\nu = \text{mod}(m, \mathcal{V})$ for $m > 0$. In explaining our sequencing strategy we shall hence refer with $\mathbf{x}_{n+\nu/\mathcal{V}}$ to particle location at $t_m = t_{n+\nu/\mathcal{V}}$.

The solution strategy proceeds by first setting up the simulation:

1. Given $\mathbf{x}_0, \mathbf{v}_0$ as samples from the initial distribution, compute $\mathbf{x}_1 = \mathbf{x}_0 + \Delta t/\mathcal{V} \mathbf{v}_0$
2. Given $\mathbf{x}_0, \mathbf{x}_1$, compute $\varrho_i^{0,1}$ from (68), solve \mathbf{e}_0 from (67), and compute $J_{j-}^{0,1}$ from (65).
3. Given $\mathbf{e}_0, \mathbf{b}_0$, solve \mathbf{b}_1 from (60)

Next we assume to be in possession of $\mathbf{e}_{n-1}, \mathbf{b}_{n-1}, \mathbf{b}_n, J_{j-}^{n-1,n}$ and $\mathbf{x}_{n-1/\mathcal{V}}, \mathbf{x}_n$, which is now obviously true for $n=1$. To advance the index n , we may proceed by following an iterative strategy:

1. Guess \mathbf{e}_n
2. Given $\mathbf{e}_n, \mathbf{b}_n$, compute \mathbf{b}_{n+1} from (60)
3. Given $\mathbf{x}_{n-1/\mathcal{V}}, \mathbf{x}_n$ compute $\mathbf{x}_{n+1/\mathcal{V}}$ using $\mathbf{e}_{n-1}, \mathbf{e}_n$ and $\mathbf{b}_{n-1}, \mathbf{b}_n, \mathbf{b}_{n+1}$ from (55).
4. Given $\mathbf{x}_n, \mathbf{x}_{n+1/\mathcal{V}}$ compute $\mathbf{x}_{n+2/\mathcal{V}}, \dots, \mathbf{x}_{n+1}$ using $\mathbf{e}_n, \mathbf{b}_n, \mathbf{b}_{n+1}$ from (55).
5. Given $\mathbf{x}_n, \dots, \mathbf{x}_{n+1}$ compute $J_{j+}^{n,n+1}$ from (64)
6. Given $J_{j-}^{n-1,n}, J_{j+}^{n,n+1}$ and $\mathbf{e}_{n-1}, \mathbf{b}_{n-1}, \mathbf{b}_n, \mathbf{b}_{n+1}$, solve \mathbf{e}_n from (63)
7. Iterate the steps 2–6 until \mathbf{e}_n converges.

Note that in performing the particle push, the expressions $b^k(t), e^j(t)$ appearing in (55) are given by (58) and (59), and similarly the particle trajectory appearing in the expressions for the current densities is the polyline (51).

E. Numerical tests

Here we summarize the results from the same numerical tests that were performed previously using the explicit scheme. Figure 4 shows the evolution of the electric energy for the two test cases as produced with the implicit subcycling scheme. The Maxwell's equation are solved with an implicit scheme. Nevertheless, the scheme is subject to a stability limit. For the one dimensional Maxwell's equation, a analysis similar to the one in²² (Appendix A.2) can be performed. This yields a stability limit of $\Delta t \leq \Delta x \sqrt{\frac{17}{14}}$ for the cubic spline finite element solver that we use in our simulations. Hence, the time step can be increased by a factor $\sqrt{3}$ compared to the explicit scheme. For the electrostatically dominated test case, we have used 1 ($\Delta t = 0.01$), 2 ($\Delta t = 0.03$), 4 ($\Delta t = 0.06$), 8 ($\Delta t = 0.12$), 16 ($\Delta t = 0.24$), 20 ($\Delta t = 0.3$), and 28 ($\Delta t = 0.43$) substeps, respectively. For the electromagnetically dominated case, we used the same number of substeps as for the explicit subcycling scheme with 8 and 12 substeps for the additional time step of $\Delta t = (0.12, 0.17)$.

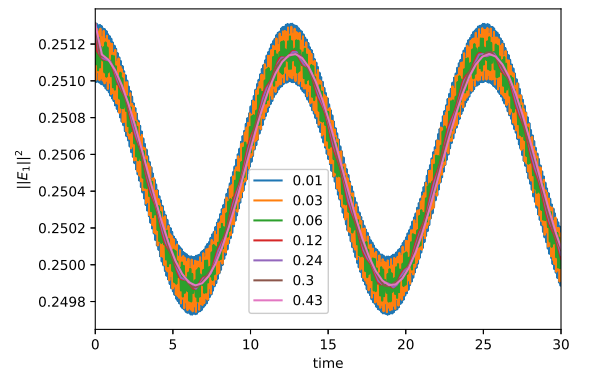
We can see that the quality of the solution is considerably improved for larger time steps in the electrostatically dominated test case. Moreover, we can see that in increasing the global time steps, the fast oscillations due to the gyromotion are not present in the solution of the implicit scheme—in contrast to the explicit subcycling scheme—and the solution follows the average motion.

Regarding computational performance, the number of Newton updates for the individual particle push is around 1.8 as in the explicit algorithm for the electromagnetically dominated case and slightly increased to about 3.3 in the electrostatically dominated case. The number of global iterations in the electromagnetically dominated case, to perform the field solves, is 2.0 for $\Delta t = (0.01, 0.03)$, 2.8 for $\Delta t = 0.06$, and 3.0 for $\Delta t = (0.09, 0.12, 0.17)$ on average. In the electrostatically dominated case, the corresponding number of global iterations is similar, namely 2.0 for $\Delta t = (0.01, 0.03)$, 2.12 for $\Delta t = 0.06$, 2.8 for $\Delta t = 0.12$, and 3.0 for $\Delta t = (0.24, 0.30, 0.43)$.

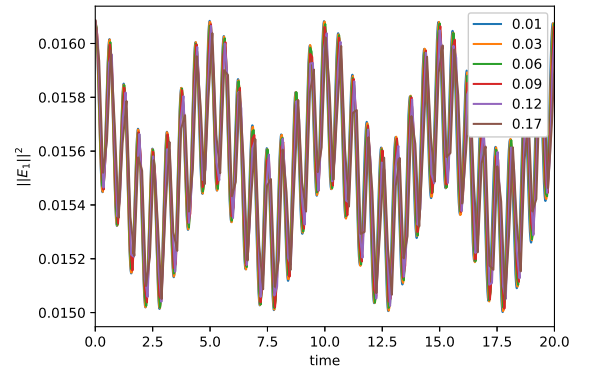
Finally, Table III shows the conservation properties of the implicit algorithm for the two test cases. We see that Gauss' law as defined in (74) is conserved to machine precision while the error in the total energy increases with respect to the increase in the global time step length but only very moderately.

V. DISCUSSION ON THE COMPUTATIONAL EFFICIENCY AND STABILITY

Finally, let us provide some insight into the computational efficiency and stability of the novel schemes, at least on a theoretical level. To properly access the performance computationally, a platform specific high-performance implementation would be necessary. Effi-



(a) Electrostatically dominated.



(b) Electromagnetically dominated.

FIG. 4: Implicit subcycling scheme: Time evolution of $\|E_1\|^2$ with various time steps (given in the legends).

cient and hardware-aware implementation of particle-in-cell codes, in particular containing integrals over intervals of varying length, is a research topic on its own and beyond the scope of this article.

The main supposed computational benefit in using a subcycling scheme, in comparison to no subcycling at all, is the fact that the global step size for the field solves can be relaxed from the step size for electrons and that the different ion species can have their own time steps characterized by the ion cyclotron timescales—one needs to be mindful of the fundamental limits set by the CFL-condition and the plasma frequency, though. In order to get an idea on the gain of the subcycling, let us assume that the total computational cost is dominated by the particle push, as it often tends to be in a particle-in-cell implementation. If we can increase the step size for all S ion species to M -times the time step of electrons, the computational complexity of the explicit subcycling method compared to the case of no subcycling at all behaves as

$$\frac{M + S}{(S + 1)M}. \quad (78)$$

With only one species of ions ($S = 1$) and eight subcycling steps ($M = 8$), the computational complexity would

Δt	Gauss' law	Energy
0.01	$9.85 \cdot 10^{-15}$	$9.29 \cdot 10^{-5}$
0.03	$1.20 \cdot 10^{-14}$	$2.19 \cdot 10^{-4}$
0.06	$1.30 \cdot 10^{-14}$	$2.81 \cdot 10^{-4}$
0.12	$1.85 \cdot 10^{-14}$	$2.11 \cdot 10^{-4}$
0.24	$2.42 \cdot 10^{-14}$	$2.29 \cdot 10^{-4}$
0.30	$2.47 \cdot 10^{-14}$	$2.46 \cdot 10^{-4}$
0.43	$3.47 \cdot 10^{-14}$	$2.01 \cdot 10^{-4}$

(a) Electrostatically dominated test case.

Δt	Gauss' law	Energy
0.01	$3.75 \cdot 10^{-15}$	$1.73 \cdot 10^{-5}$
0.03	$4.80 \cdot 10^{-15}$	$4.20 \cdot 10^{-5}$
0.06	$6.40 \cdot 10^{-15}$	$7.59 \cdot 10^{-5}$
0.09	$7.03 \cdot 10^{-15}$	$1.14 \cdot 10^{-4}$
0.12	$7.18 \cdot 10^{-15}$	$1.51 \cdot 10^{-4}$
0.17	$6.29 \cdot 10^{-15}$	$2.20 \cdot 10^{-4}$

(b) Electromagnetically dominated test case.

TABLE III: Implicit subcycling scheme: Conservation laws for different time steps.

be reduced to 0.56 times the original, already close to the ideal 0.5. If the number of ion species is increased to $S = 4$, the computational complexity is reduced to 0.3 times the original. This means that the explicit subcycling scheme has excellent potential to reduce the computational complexity in simulations of multiple species in magnetized plasmas. This observation is emphasized by the fact that the modifications introduced by the explicit subcycling scheme to the existing variational methods are minimal.

Analysis of the implicit scheme is not that much different of that of the explicit scheme: the field solve requires an iterative approach which increases the number of necessary evaluations of the particle orbits by a factor of I and provides a new estimate for the relative complexity

$$\frac{I(M + S)}{(S + 1)M}. \quad (79)$$

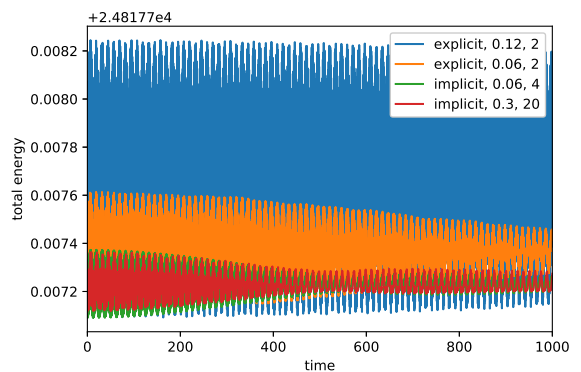
For example, in the electrostatically dominated simulation with the global step of $\Delta t = 0.30$ we had to evaluate 3 fixed-point iterations on average, while the number of subcycling steps was set to 20. Assuming only one ion species, the complexity of the implicit scheme would be 1.58, but with 4 ion species, this would be reduced to 0.72 already. Hence the more there are ion species to simulate, the more efficient the implicit scheme becomes.

Additionally, the subcycling in both the explicit and the implicit scheme has the advantage that all substeps can be performed at once for each particle. This way the arithmetic intensity of the algorithms is increased which should render the algorithm to behave favorably on modern computer architecture. Assessing this property thoroughly would, however, require high-performance implementations of the methods.

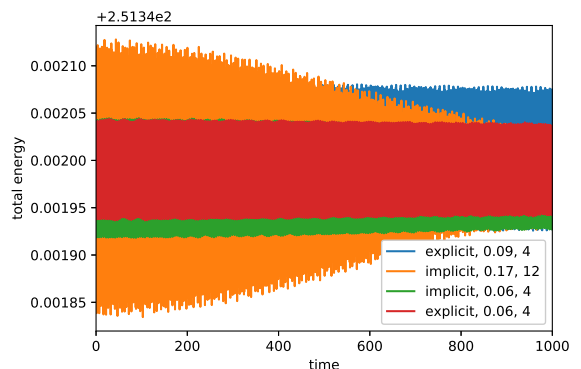
Regarding the performance of the algorithms in long-time simulations, variational methods (and the Hamil-

tonian splitting schemes) in general are the best tools available. This is typically merited to the conservation of the multisymplectic two-form and the good behaviour of energy in the sense that it is bounded with the bounds depending on the time step size. The analyses are typically performed for synchronous integrators, but examples exist also for asynchronous variational integrators²⁵. We anticipate that the analysis could be extended also to our subcycling schemes but this is left to a future study.

It would likely be possible to perform also the so-called backwards error analysis using the flow maps of the numerical schemes to find a Taylor series expression for the Hamiltonian the discrete flow map conserves exactly. This procedure has been left for future analysis, though, for we expect it to be somewhat more complicated a procedure than the backwards error analysis of synchronous integrators. Instead, we have simply run some of the simulations over prolonged intervals, corresponding to 1000.0 time units. Figure 5 shows the time evolution of the total energy which demonstrates the typical behavior for variational integrators: the energy is oscillating, displaying multiple different frequencies, but remains bounded nevertheless.



(a) Electrostatically dominated.



(b) Electromagnetically dominated.

FIG. 5: Evolution of the total energy over 1000 time units with the explicit and implicit field solve and varying number of $\Delta t, \nu$ as given in the legend.

VI. SUMMARY

In this paper, we have introduced two possible sub-cycling algorithms for variational GEMPIC methods addressing the Vlasov–Maxwell system in magnetized plasmas. The first one is a straightforward upgrade of the existing variational GEMPIC methods, specifically of the one given in¹. The algorithm was tested both in electrostatically and electromagnetically dominated cases. The tests revealed that the resulting, rather peculiar sub-cycling scheme—magnetic field is properly orbit-averaged but the electric-field impulse evaluated only once per the sub-cycling period—may result in artificial oscillations if the electric field impulse is too strong in relation to the magnetic field impulse. The root cause was verified by enforcing the electric-field orbit averaging which removed the spurious oscillations but resulted in a non-variational particle push. We have performed also low-resolution 3-D simulations and the results remain qualitatively the same.

Our second algorithm is aimed at solving the possible limitations of the first algorithm. Instead of relying on the “summation-by-parts” trick, which is the cornerstone of the existing electromagnetically gauge-invariant variational GEMPIC methods, we considered the possibility of performing genuine integration by parts instead. This led us to suggest an algorithm where the orbit-averaging is done properly for both the electric and magnetic impulse and which retains the gauge invariance and hence the algebraic charge-conservation law. Numerical tests confirmed our hypothesis, and the artificial oscillations vanished. The trade-off with the second algorithm is that it requires a global implicit solve for the electric field, the current density, and the particle push are entangled. Furthermore, it appears to be difficult to find an explicit one for it seems to be necessary to treat the electromagnetic potential as being time-continuous for the sake of performing partial integrations in the field-particle-interaction part of the discrete action and this tightly couples the degrees of freedom for the fields to the degrees of freedom for the particles during the synchronizing global steps, effectively resulting in a globally implicit scheme. The non-synchronous particle steps fortunately remain decoupled and lead to only individually implicit push like in the semi-explicit algorithm.

It remains to be seen whether sub-cycling of particle orbits in explicit, variational geometric particle-in-cell methods with proper orbit-averaging of both electric and magnetic impulses is possible. In the future, we aim to investigate also the possibility of adaptive temporal integration. Such algorithm would be ideal from the perspectives that the guiding magnetic field may vary spatially. For example in ITER fusion device, the inboard magnetic field strength will be approximately 7 T while the outboard side will be at 4 T.

DATA AVAILABILITY STATEMENT

The data that support the findings of this study has been generated with the SeLaLib computer library²³.

ACKNOWLEDGMENTS

Financial support for the work of E.H. and F.Z. was provided by the Academy of Finland grant Nos. 315278 and 320058. Work of K.K. has been carried out within the framework of the EUROfusion Consortium and has received funding from the Euratom research and training programme 2014–2018 and 2019–2020 under grant agreement No 633053. The views and opinions expressed herein do not necessarily reflect those of the European Commission, Academy of Finland, or Aalto University.

- ¹J. Squire, H. Qin, and W. M. Tang, “Geometric integration of the Vlasov-Maxwell system with a variational particle-in-cell scheme,” *Physics of Plasmas* **19**, 084501 (2012), arXiv:1401.6723.
- ²E. G. Evstatiev and B. A. Shadwick, “Variational formulation of particle algorithms for kinetic plasma simulations,” *Journal of Computational Physics* **245**, 376–398 (2013), arXiv:1210.3743.
- ³B. A. Shadwick, A. B. Stamm, and E. G. Evstatiev, “Variational formulation of macro-particle plasma simulation algorithms,” *Physics of Plasmas* **21**, 055708 (2014).
- ⁴A. B. Stamm, B. Shadwick, and E. G. Evstatiev, “Variational Formulation of Macroparticle Models for Electromagnetic Plasma Simulations,” *IEEE Transactions on Plasma Science* **42**, 1747–1758 (2014).
- ⁵J. Xiao, H. Qin, J. Liu, Y. He, R. Zhang, and Y. Sun, “Explicit high-order non-canonical symplectic particle-in-cell algorithms for Vlasov-Maxwell systems,” *Physics of Plasmas* **22**, 112504 (2015), arXiv:1510.06972.
- ⁶Y. He, H. Qin, Y. Sun, J. Xiao, R. Zhang, and J. Liu, “Hamiltonian time integrators for Vlasov-Maxwell equations,” *Physics of Plasmas* **22**, 124503 (2015), arXiv:1505.06076.
- ⁷H. Qin, J. Liu, J. Xiao, R. Zhang, Y. He, Y. Wang, Y. Sun, J. W. Burby, L. Ellison, and Y. Zhou, “Canonical symplectic particle-in-cell method for long-term large-scale simulations of the Vlasov-Maxwell equations,” *Nuclear Fusion* **56**, 014001 (2016), arXiv:1503.08334.
- ⁸J. Xiao, H. Qin, P. J. Morrison, J. Liu, Z. Yu, R. Zhang, and Y. He, “Explicit high-order noncanonical symplectic algorithms for ideal two-fluid systems,” *Physics of Plasmas* **23**, 112107 (2016), arXiv:1606.07005.
- ⁹M. Kraus, K. Kormann, P. J. Morrison, and E. Sonnendrücker, “GEMPIC: geometric electromagnetic particle-in-cell methods,” *Journal of Plasma Physics* **83**, 905830401 (2017), arXiv:1609.03053.
- ¹⁰J. Xiao, H. Qin, and J. Liu, “Structure-preserving geometric particle-in-cell methods for Vlasov-Maxwell systems,” *Plasma Science and Technology* **20**, 110501 (2018), arXiv:1804.08823.
- ¹¹J. Xiao and H. Qin, “Explicit Structure-Preserving Geometric Particle-in-Cell Algorithm in Curvilinear Orthogonal Coordinate Systems and Its Applications to Whole-Device 6D Kinetic Simulations of Tokamak Physics,” arXiv e-prints, arXiv:2004.08150 (2020), arXiv:2004.08150.
- ¹²P. J. Morrison, “Structure and structure-preserving algorithms for plasma physics,” *Physics of Plasmas* **24**, 055502 (2017), arXiv:1612.06734.
- ¹³J. C. Adam, A. G. Serveniére, and A. B. Langdon, “Electron Sub-Cycling in Particle Simulation of Plasma,” *Journal of Computational Physics* **47**, 229–244 (1982).

- ¹⁴B. I. Cohen, “10 - orbit averaging and subcycling in particle simulation of plasmas,” in *Multiple Time Scales*, edited by J. U. Brackbill and B. I. Cohen (Academic Press, 1985) pp. 311 – 333.
- ¹⁵S. Markidis, G. Lapenta, and Rizwan-uddin, “Multi-scale simulations of plasma with iPIC3D,” *Mathematics and Computers in Simulation* **80**, 1509 – 1519 (2010), Multiscale modeling of moving interfaces in materials.
- ¹⁶G. Chen, L. Chacón, and D. C. Barnes, “An energy- and charge-conserving, implicit, electrostatic particle-in-cell algorithm,” *Journal of Computational Physics* **230**, 7018–7036 (2011).
- ¹⁷L. Chacón, G. Chen, and D. C. Barnes, “A charge- and energy-conserving implicit, electrostatic particle-in-cell algorithm on mapped computational meshes,” *Journal of Computational Physics* **233**, 1–16 (2013).
- ¹⁸G. Chen and L. Chacón, “An energy- and charge-conserving, nonlinearly implicit, electromagnetic 1D–3V Vlasov–Darwin particle-in-cell algorithm,” *Computer Physics Communications* **185**, 2391–2402 (2014).
- ¹⁹I. B. Peng, S. Markidis, A. Vaivads, J. Vencels, J. Amaya, A. Divin, E. Laure, and G. Lapenta, “The Formation of a Magnetosphere with Implicit Particle-in-Cell Simulations,” *Procedia Computer Science* **51**, 1178 – 1187 (2015), International Conference On Computational Science, ICCS 2015.
- ²⁰L. Chacón and G. Chen, “A curvilinear, fully implicit, conservative electromagnetic PIC algorithm in multiple dimensions,” *Journal of Computational Physics* **316**, 578–597 (2016).
- ²¹G. Chen, L. Chacón, L. Yin, B. J. Albright, D. J. Stark, and R. F. Bird, “A semi-implicit, energy- and charge-conserving particle-in-cell algorithm for the relativistic Vlasov–Maxwell equations,” *Journal of Computational Physics* **407**, 109228 (2020), arXiv:1903.01565.
- ²²K. Kormann and E. Sonnendrücker, “Energy-conserving time propagation for a geometric particle-in-cell Vlasov–Maxwell solver,” (2019), arXiv:1910.04000.
- ²³“SeLaLib,” <http://selalib.gforge.inria.fr/>.
- ²⁴J. Bernier, F. Casas, and N. Crouseilles, “Splitting methods for rotations: application to vlasov equations,” (2019), working paper or preprint.
- ²⁵A. Lew, J. E. Marsden, M. Ortiz, and M. West, “Asynchronous Variational Integrators,” *Archive for Rational Mechanics and Analysis* **167**, 85–146 (2003).